Numerical and Experimental Investigation of heat transfer and flow structures around three heated spheres in tandem arrangement

A H Abed[1, 2], S E Shcheklein[1] and V M Pakhaluev[1]

[1]Ural Federal University named after the first President of Russia B. N. Yeltsin 19 Mira St., Yekaterinburg, 620002, Russia
[2]Department of Electromechanical Engineering, University of Technology, Al-Sina'a St., Baghdad, 10066, Iraq

E-mail: akraaam82@yahoo.com

Abstract. The objective of this work is to evaluate the convective heat transfer and flow characteristics around three heated spheres in a tandem arrangement. Numerical simulation and Experimental verification were performed using stationary copper spheres located inside a cylindrical channel with constant channel-to-sphere diameter ratio. Numerical simulation is done for three-dimensional steady-state flow using ANSYS-FLUENT by solving the Reynolds-Averaged Navier Stokes (RANS) equations. Over the test range of Reynolds numbers (2500-55000), the numerical results of the average surface temperature and heat transfer coefficient obtained are a reasonably good agreement with those obtained by experimental measurements. The distributions of the heat transfer coefficient, temperature profiles, velocity field and pressure coefficient around the sphere's surface are calculated and analyzed.

1. Introduction

The heat transfer and flow structure passing around multiple heated bluff bodies are widely investigated problems due to their importance in several engineering such as high temperature gas-cooled nuclear reactor - HTGR [1], bio-film reactor [2] and solar receivers [3], etc. applications such as nuclear power plants, food and chemical processing, and so on. The flow separation complexity and the vortex shedding mechanisms, generated by the sphere arrays have attracted large attention. In the literature, numerical and experimental investigations have been conducted to analyze and understand the wake flow structure around a single-sphere and various arrangements of two spheres [4-7]. In the early studies, Achenbach [8] experimentally investigated the vortical structure of a single sphere wake in the Reynolds number range of 5 x 104 ≤ Re ≤6 x 106. Also, the local static pressure and the skin friction were measured to evaluate the flow separation angle. Sakamoto et al. [9] visualized the wake structure behind a single sphere using dye, and then the vortex shedding was measured by the hot-wire technique. The computational fluid dynamics (CFD) simulation allows an important approach, in which the packing sphere is fully simulated. For example in space between the spheres all local values of relevant variables, such as velocity field, pressure drop, temperature profiles, and so on, is determined by solving the Navies Stokes equations. Such parameters considered to be important details to predict and understanding of the phenomena that occur in such packed spheres. A little investigation has been performed to study the heat transfer and the interaction of the wakes of two spheres in tandem, transverse and staggered arrangements. The Drag force, flow patterns transition and wake structure of two

interactive spheres were analyzed experimentally and numerically by Chen et al. [10] and Zou et al. [11]. Laser flow visualization has been used to determine the flow separation angle and identify the effect of aligned angle between two spheres. They indicated that the wake structure of a sphere was more affected by the distance and the aligned angle between spheres. Zhang et al. [12] numerically investigated the effect of spacing between two vertically arranged spheres on natural heat transfer for $2 \leq S/D \leq 24$. They noticed that the re-circulation zone is seriously affecting on the convective heat transfer coefficient and as the spacing ratio between two separate spheres increases about 24 times of the sphere diameter, the flow re-circulation zone takes place over the upper sphere for circumferential angle $142.5° \leq \theta \leq 180°$. In the sphere swarms for most engineering and practical applications, the data of the single sphere is not capable to precisely predicate the mass transfer process [8]. Juncu [13, 14] solved numerically the mass transfer between two spheres have the same diameter in the tandem arrangement and incompressible moving fluid. This work aims to extend the analysis of the heat transfer, boundary layer development and flow structure of three interactive spheres under a steady-state condition. The spheres were packed inside the cylindrical channel with a constant channel-to-sphere diameter ratio. The influence of the generated vortices on heat transfer performance and moving flow structure are examined. In order to validate the CFD simulation method, the CFD results were compared with those obtained by experimental measurements.

2. Physical model and CFD Simulation conditions

The computational domain geometry and mesh models for CFD simulation are shown in figure 1. The test spheres are located inside a vertical cylindrical channel in a tandem arrangement with the constant channel-to-sphere D/d ratio.
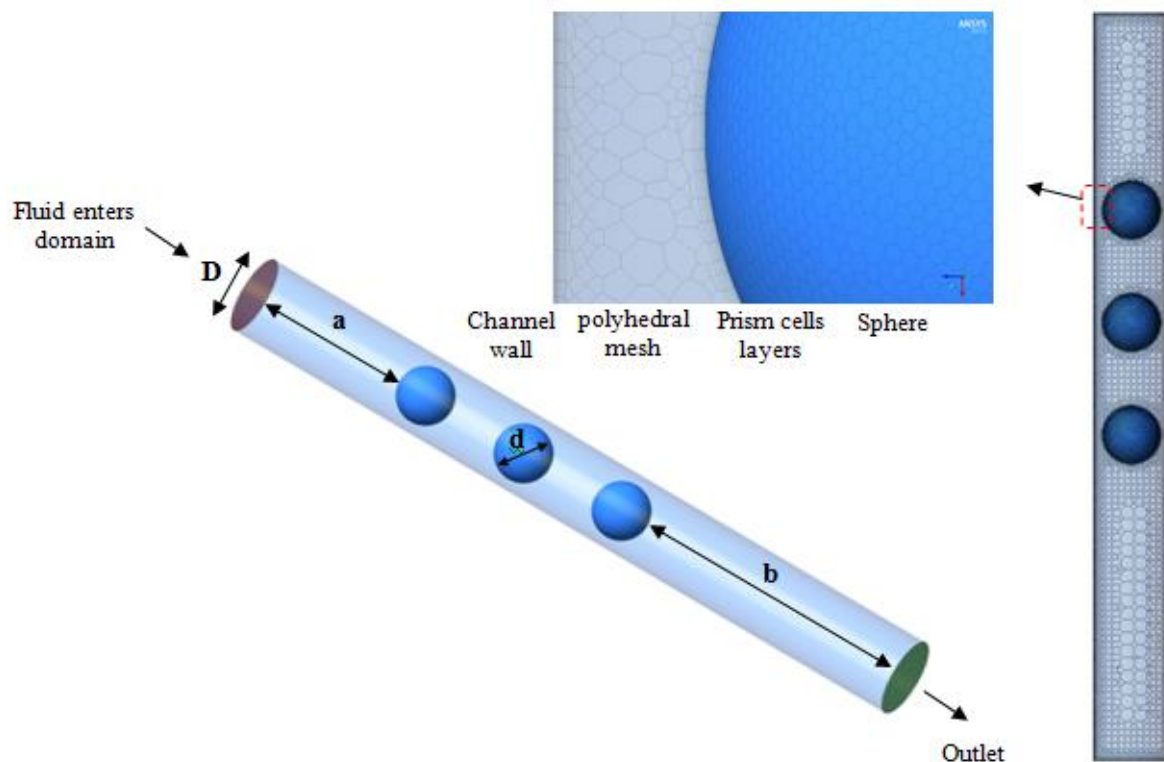

Figure 1. Schematic view of the computational domain geometry and mesh models for CFD simulation.

The computational domain consists of the inlet region, 3 layers of full spheres and an outlet region. The air was used as working fluid and the velocity and temperature at the inlet region were kept at Ti and ui, respectively. In addition, an opening boundary with a constant average static pressure was applied at the outlet region. In the present study, the computational domain is discretized into the fluid region as well as a solid region uses 1.8 million cells and 0.4 million cells for the fluid and solid regions, respectively. Due to the complicated geometry of the flow domain including the gaps region (equal ds) between the spheres, unstructured mesh with tetrahedral cells are adopted for computational domain and then transformed into polyhedral cells in Ansys fluent to enhance the numerical stability of the model. The commercial software ANSYS FLUENT version 17 was used in this work. Governing equations for CFD simulations are as follow [15].

Continuity equation

$$\frac{\partial}{\partial x_i}\left(\rho u_i\right) + \frac{\partial}{\partial x_j}\left(\rho u_j\right) + \frac{\partial}{\partial x_k}\left(\rho u_k\right) = 0 \tag{1}$$

Momentum equation

$$\frac{\partial(\rho u_i u_i)}{\partial x_i}\left(\rho u_i\right) + \frac{\partial(\rho u_i u_j)}{\partial x_j}\left(\rho u_j\right) + \frac{\partial(\rho u_i u_k)}{\partial x_k}\left(\rho u_k\right) =$$
$$= -\frac{\partial p}{\partial x_i} + \frac{\partial(\tau_{ii})}{\partial x_i} + \frac{\partial(\tau_{ij})}{\partial x_j} + \frac{\partial(\tau_{ik})}{\partial x_k} + \rho g_i + F_i \tag{2}$$

Energy equation

$$\frac{\partial(\rho uT)}{\partial x_i} + \frac{\partial(\rho vT)}{\partial x_j} + \frac{\partial(\rho wT)}{\partial x_k} = \frac{\partial}{\partial x_i}\left(\frac{k}{c_p}\frac{\partial T}{\partial x_i}\right) + \frac{\partial}{\partial x_i}\left(\frac{k}{c_p}\frac{\partial T}{\partial x_j}\right) + \frac{\partial}{\partial x_i}\left(\frac{k}{c_p}\frac{\partial T}{\partial x_k}\right) \tag{3}$$

The SST k-ω turbulence model which combines the advantages of the k-ε and k-ω models were applied in this simulation and the scalable wall-function treatment with an appropriate dimensionless distance of the wall grid elements (y+) were adopted. The SST k-ω model can be described as follows [15]:

Kinematic Viscosity

$$v_k = \frac{a_1\kappa}{\max\left(a_1\omega, SF_2\right)} \tag{4}$$

Turbulence Kinetic Energy

$$\frac{\partial\kappa}{\partial t} + U_j\frac{\partial\kappa}{\partial x_j} = P_\kappa - \beta^*\kappa\omega + \frac{\partial}{\partial x_j}\left[\left(v + \sigma_k v_k\right)\cdot\frac{\partial\kappa}{\partial x_j}\right] \tag{5}$$

Specific turbulence dissipation rate

$$\frac{\partial\omega}{\partial t} + U_j\frac{\partial\omega}{\partial x_j} = \alpha S^2 - \beta\omega^2 + \frac{\partial}{\partial x_j}\left[\left(v + \sigma_\omega v_k\right)\frac{\partial\omega}{\partial x_j}\right] + 2\left(1 - F_1\right)\sigma\omega^2\frac{1}{\omega}\frac{\partial\kappa}{\partial xi}\frac{\partial\omega}{\partial xi} \tag{6}$$

3. Experimental Setup and Procedure

The experimental setup details are depicted schematically in figure 2. In the experimental setup, the inlet working fluid was directed to the heated spheres by 1000 W air pump. Using the pitot tube with a

digital manometer calibrated by a vane-type anemometer, the airflow rate was measured. The airflow rate was controlled by modifying the pump speed through a variac voltage regulator. The test objects are copper spheres having 34mm diameter were heated independently using 100W - electrical heater with a variac transformer to obtain a uniform heat flux. The test spheres were packed inside an adiabatic cylindrical channel in tandem arrangement with constant pitch ratio (p=ds). For each sphere, two k-type thermocouples were used to directly measure the surface temperature (Tw), were embedded in points referred by the numbers 1, 2 as shown in figure. 2. Further, the inlet and outlet air temperatures were recorded using two thermocouples located immediately in the air entrance region and outlet region of the adiabatic channel. After reaching the steady-state condition, all the temperatures were recorded by using MSD200 data logger.
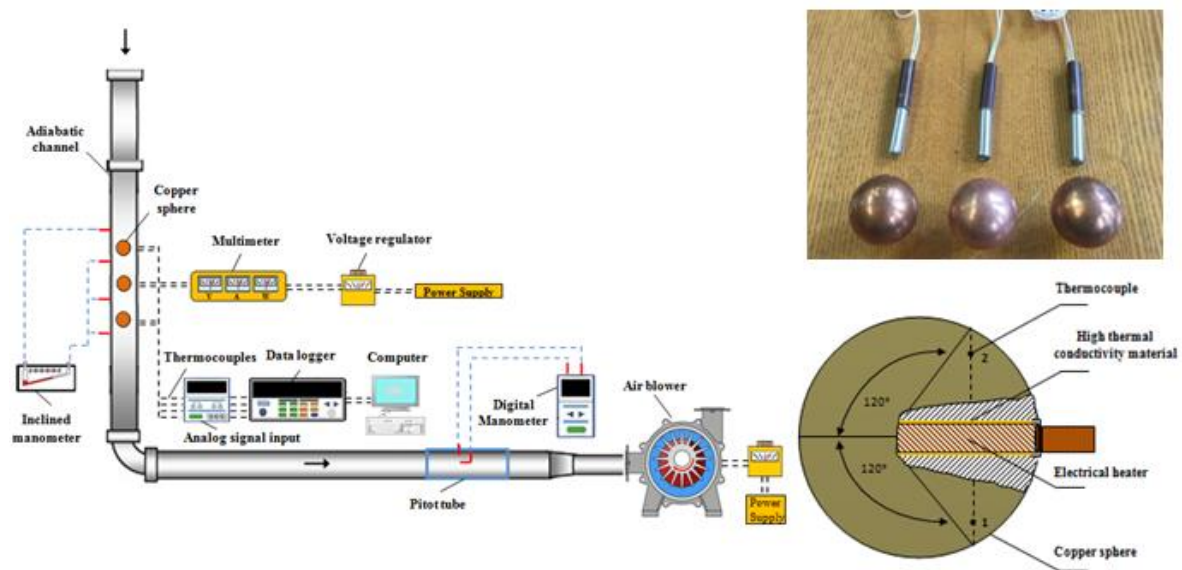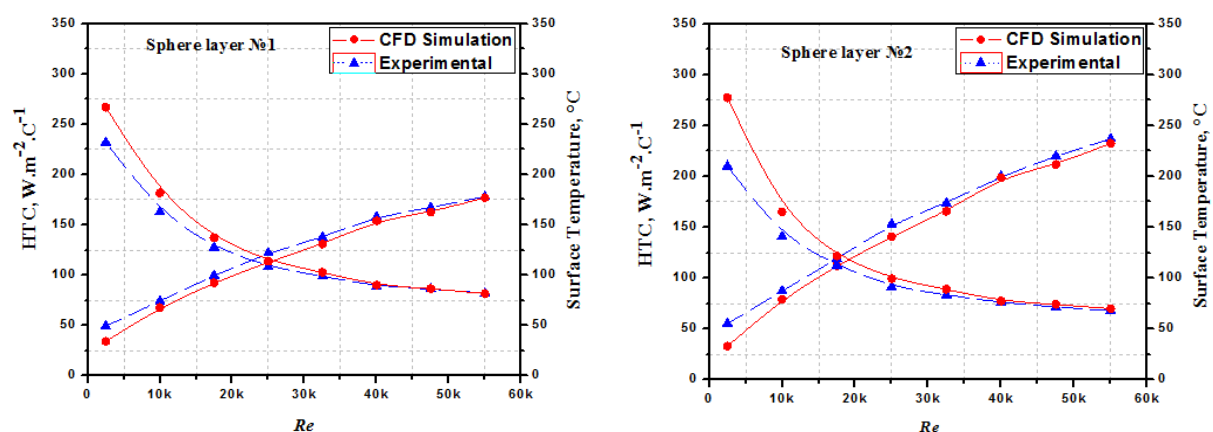

Figure 2. Schematic diagram of the experimental Setup and the construction of heat transfer models.

4. Results and discussion

Herein, the simulation results of the spheres packing inside a vertical cylindrical channel in a tandem arrangement were described and the performed experimental results are presented. First, the numerical results of the average surface temperature and heat transfer coefficient obtained from the present simulation are compared with those obtained by experimental measurements as shown in figure 3. The average deviations of the present results are within 5.8%, 6.1%, and 7.5%, respectively.
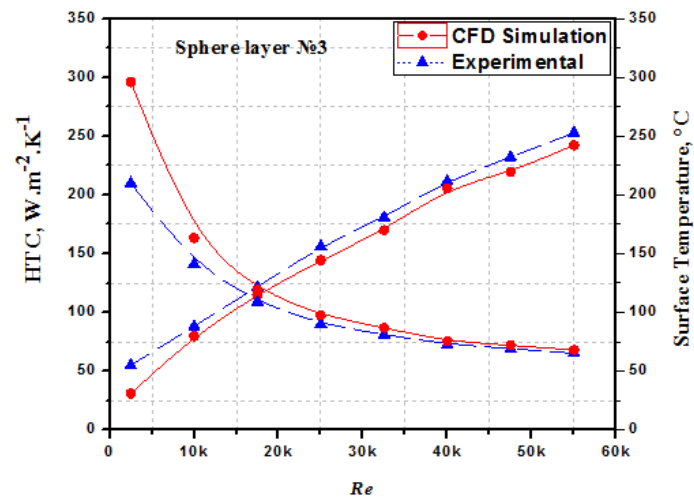
Figure 3. Comparison of average surface temperature and heat transfer coefficient.

It can be observed that the average surface temperature tends to decrease and the heat transfer coefficient tends to increase with increasing of Re for all spheres layers. With the help of the experimental measurements, the experimental results of average Nusselt number are correlated as shown in Eq. (4) below.

$$Nu = C_i \, Re^{0.58} \, Pr^{0.33}$$

where Ci is the constant in the heat transfer rate correlation with $C_1 = 0.47$; $C_2 = 0.65$, and $C_3 = 0.69$.
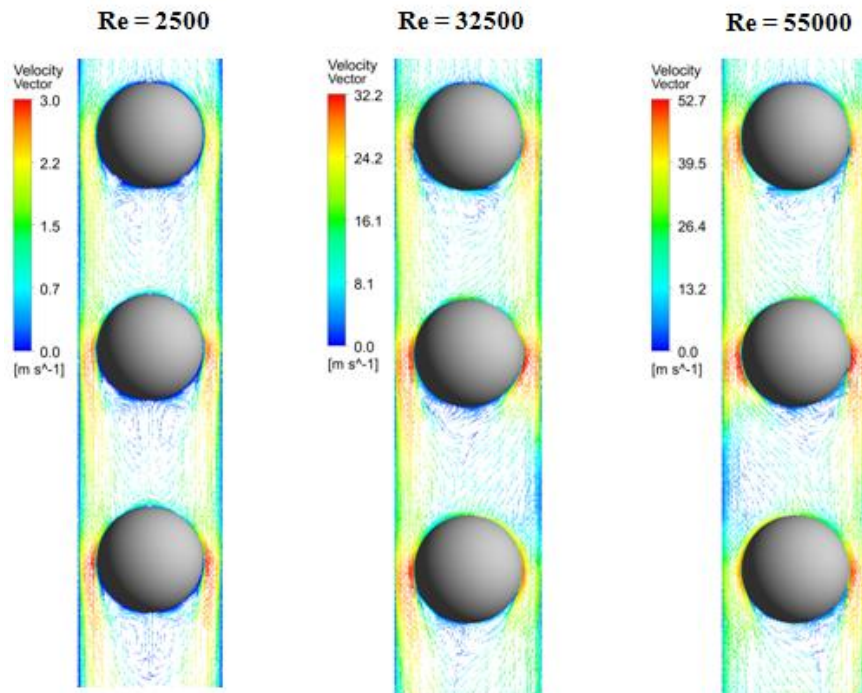

Figure 4. Velocity streamlines around spheres: Re=2500 Re=32500 and Re=55000.

Figure. 4 depicts the flow streamlines characteristics among the spheres layer. The color index represents the magnitude of the velocity at any point. The air flows through the sphere structure and it can be seen that the streamline distribution around the second and third layers are different from those in the first layer. Within the sphere gaps, the airflow was accelerated and leads to increasing of the turbulence intensity imparted to the flow at the sphere surface. In the front region on each sphere surface of the second and third layers, there are a number of accelerating points that may improve the heat transfer rate. From the numerical and experimental results in figure 5, it is observable that the second and third layers yield considerable heat transfer in comparison with the first layer due to the increase of turbulence intensity.
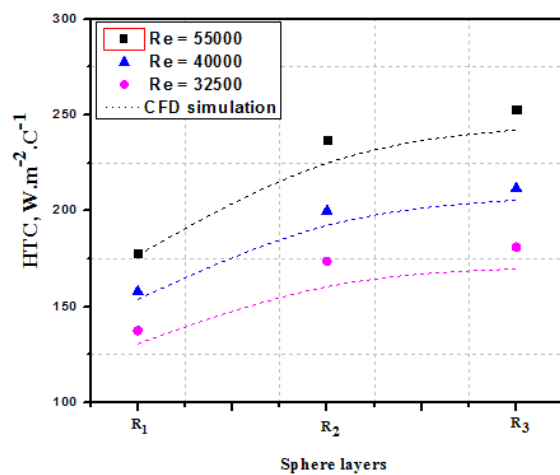

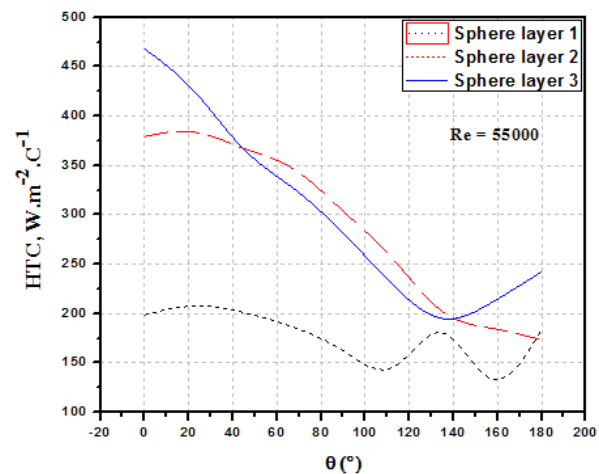**Figure 5.** Variations of average heat transfer co-efficient as a function of sphere layers.

Figure 6. Variations of average heat transfer coefficient as a function of angle measured from stagnation point.
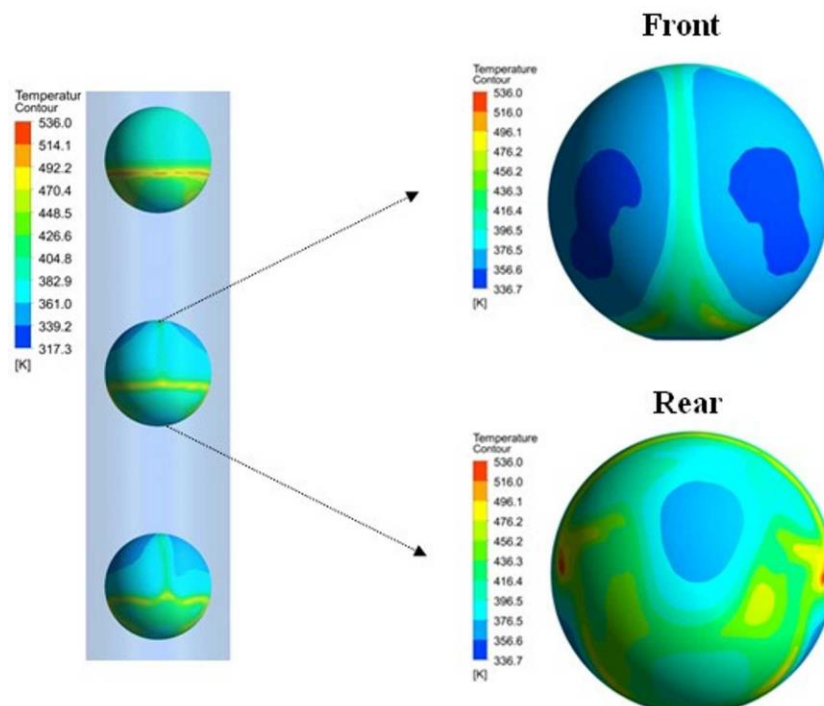

Figure 7. Temperature contours of a selected sphere.

The local heat transfer coefficient as a function of the angle [θ] measured from the front stagnation point is shown in figures 6, for Reynolds number (Re=55000). For the present data, the heat transfer coefficient for the second and third layers around 63–72% higher than the first layer. Figure 7 represents the calculated temperature distribution on both the front and rear regions of the selected sphere and its cross-section. The color index represents the magnitude of the local temperature. From this figure, it is obvious that the heat transfer rate in the front region is higher with comparison to the condition in the rear region due to the high turbulence intensity leading to enhance the convection heat transfer than the rear region as we mentioned above. The variations of pressure coefficient (Cp) for all spheres layer as a function of zenith angle are shown in figure. 8. It can be noticed that the pressure coefficient on the front-upper region ($\theta = 0°$ to $60°$) of the sphere is positive and that on the lower-front and upper-rear area is negative.
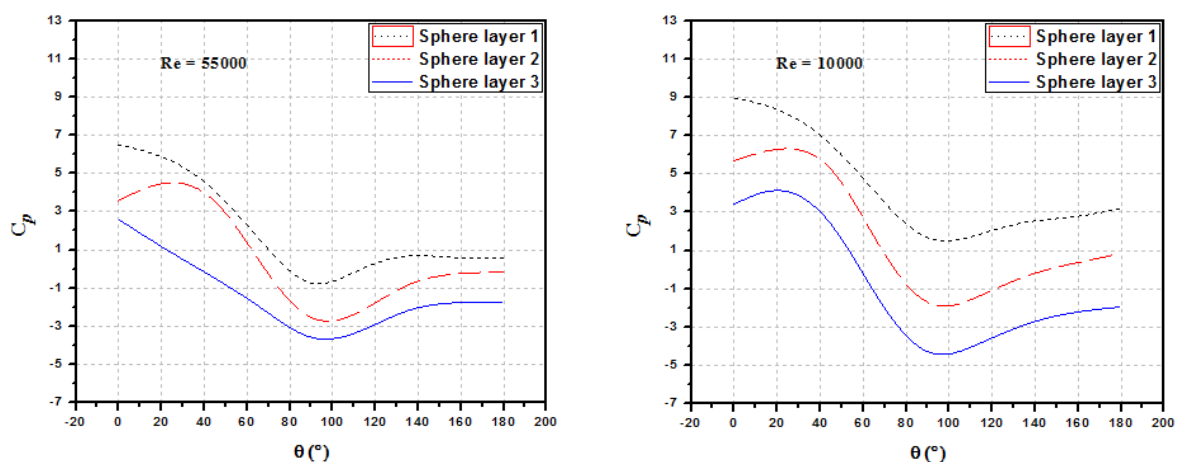

Figure 8. Pressure coefficient distribution as function of angle measured from stagnation point.

5. Conclusions

Numerical and experimental investigation of heat transfer characteristics and flow structures around three heated spheres in a tandem arrangement for Re numbers ranges 2500-55000 has been performed. The highest heat transfer rate is found at the second and third layers due to airflow accelerated that leads to increasing of the turbulence intensity imparted to the flow at the sphere's surface. The heat transfer coefficient for the second and third layers around 63–72% higher than the first layer. Additionally, the new empirical correlation for the Nusselt number based on the experimental data is proposed. The agreement between the numerical results and those obtained from the experimental measurements is reasonable.

References

[1]   Filippov G, Bogoyavlenskii R, Ponomarev-Stepnoi N and Gol'tsev A 2004 Vy`sokotemperaturny`j gelievy`j modul`ny`j yaderny`j reaktor s sharovy`mi TVE`Lami dlya proizvod-stva e`lektroe`nergii i vodoroda [Modular High-Temperature Helium-Cooled Nuclear Reactor with Spherical Fuel Elements for Electricity and Hydrogen Production] Atomnaya e`nergiya [*Atomic Energy*] **96(3)** 152-8
[2]   Fan C and Wang H 2012 Degradation of Methyl Paraben by the Aerated Pebble-bed Biofilm System *APCBEE Procedia* **1** 299-303
[3]   Lu JF, Chen Y, Ding J, Wang WL 2016 High temperature energy storage performances of me-thane reforming with carbon dioxide in a tubular packed reactor *Appl Energ* **162** 1473-82
[4]   Ozgoren M 2013 Flow structures around an equilateral triangle arrangement of three spheres *Int. J. of Multiphase Flow* **53** 54-64

[5]   Peng X and Huang G 2017 Effect of temperature difference on the adhesive contact between two spheres *Int. J. of Engineering Science* **116** 25-34

[6]   Tsutsui T 2008 Flow around a sphere in a plane turbulent boundary layer *J. of Wind Engineering and Industrial Aerodynamics* **96(6-7)** 779-92

[7]   Nagata T, Nonomura T, Takahashi S, Mizuno Y and Fukuda K 2018 Direct numerical simulation of flow around a heated/cooled isolated sphere up to a Reynolds number of 300 under subsonic to supersonic conditions *Int. J. of Heat and Mass Transfer* **120** 284-99

[8]   Achenbach E 1972 Experiments on the flow past spheres at very high Reynolds numbers *J. of Fluid Mechanics* **54(3)** 565-75

[9]   Sakamoto H and Haniu H 1990 A Study on Vortex Shedding From Spheres in a Uniform Flow *J. of Fluids Engineering* **112(4)** 386

[10]   Chen R and Wu J 2000 The flow characteristics between two interactive spheres *Chemical Engineering Science* **55(6)** 1143-58

[11]   Zou J, Ren A and Deng J 2005 Study on flow past two spheres in tandem arrangement using a local mesh refinement virtual boundary method *Int. J. for Numerical Methods in Fluids* **49(5)** 465-88

[12]   Zhang J, Zhen Q, Liu J and Lu W 2019 Effect of spacing on laminar natural convection flow and heat transfer from two spheres in vertical arrangement *Int. J. of Heat and Mass Transfer* **134** 852-65

[13]   Juncu Gh 2007 Unsteady forced convection heat/mass transfer around two spheres in tandem at low Reynolds numbers *Int. J. Thermal Sci.* **46** 1011-22

[14]   Juncu Gh 2018 Mass transfer from two spheres in tandem accompanied by chemical reactions *Chemical Engineering Science* **189** 102-13

[15]   Fluent Inc. 2005 Fluent 6.2 User *Manual*